UNCLASSIFIED

AD **402 819**

Reproduced
by the

DEFENSE DOCUMENTATION CENTER

FOR

SCIENTIFIC AND TECHNICAL INFORMATION

CAMERON STATION, ALEXANDRIA, VIRGINIA

UNCLASSIFIED

(4) NA

T 10

(1)

(6) STUDIES OF THERMAL PLASMAS ASSOCIATED

WITH HYPERSONIC RE-ENTRY CONDITIONS

(7 NA)

(8) (U)

(9) SEMI-ANNUAL REPORT

402 819

(10) NA

(11) Mar 63

October 1962 - March 1963

(12) IV.

(13) CAL

(14) NA

ARPA Order Number: 322 Amendment #2

Project Code Number: 3740

Name of Contractor: Cornell Aeronautical Laboratory, Inc., Buffalo, N Y.

Date of Contract: 24 September 1962

Amount of Contract: $65,000.00

(15) Contract Number: Nonr 3960(00)

Contract Expiration Date: 23 September 1963

Project Engineer and Phone Number: John Daiber
716-NF-2-7500

(16-19 NA)

(20) (U)

(35) 227800

402819

ASTIA FILE COPY 402819

AD NO.

ABSTRACT

This report summarizes the progress made on a program to study
the thermal plasmas associated with hypersonic re-entry. One of the
major contributors to the ionization level in the gas sheath of re-entry
vehicles is the nitric oxide ion. The primary reaction for this ion is the
dissociative recombination reaction, $NO^+ + e^- \longrightarrow N + O$. This reaction
rate was measured in the CAL six-foot low-density shock tunnel by mon-
itoring the electron density with X- and S-band microwave interferometers.
A recombination rate was then fitted to the data by using the nonequilibrium
nozzle flow computational program developed at CAL. The tentative results
indicate that the dissociative recombination reaction rate for NO^+ is
$3 \times 10^{20} \, T^{-1.5}$ cc/mole-sec with an uncertainty factor of two. The meas-
ured electron collision frequencies were higher than those predicted. There-
fore, additional shock tube experiments are in progress to measure the
collision cross-section of air species to thermal electrons by using X-band
microwave diagnostics in an equilibrium plasma.

TABLE OF CONTENTS

LIST OF ILLUSTRATIONS

INTRODUCTION

The purpose of this research program is to study the thermal plasmas associated with hy,ersonic re-entry conditions. This Semi-Annual Report presents the progress under the present contract for the period of October 1962 through March 1963, which constitutes the first half year of this effort. The investigation can conveniently be divided into two areas. One deals with the determination of the electrical properties of the non-equilibrium plasma sheath. The other phase deals with the interaction of these plasmas with radio-frequency electromagnetic signals.

Section I of this report deals with deionization rate constant measurements in air. The determination of these rates will then allow more accurate calculation of the electron density in the flow field of re-entry bodies. The reduction and interpretation of the data obtained. so far have been completed. However, the conclusions are still tentative because of the disagreement between measured and predicted electron collision frequencies.

Sections II and III deal with the interaction of microwaves with a thermal plasma. The experiment in progress is described in Section II. Its objective is to perfect the microwave transmission measurements as a diagnostic tool for studying the perturbation of a plasma by strong radio-frequency interactions. To verify this diagnostic method, measurements will be made in this coming half year of the collision cross-sections of O_2, N_2, O and possibly N and NO to thermal electrons. These results will be useful for interpreting the collision frequency data in

Section I and for predicting the effect of re-entry plasma sheaths on communications.

In Section III a short description is given of the present plans for studying the interaction of strong signals with a thermal plasma.

I. NO$^+$ DISSOCIATIVE RECOMBINATION REACTION-RATE MEASUREMENTS

For vehicle re-entry at sub-orbital velocities ($<$ 23,000 fps) the
ionization levels in the plasma sheath can be adequately calculated by con-
sidering only one charged species,[1] NO$^+$. The most important reaction
path for this species is the dissociative recombination

$$NO^+ + e \longrightarrow N + O$$
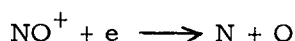
It is therefore important that this reaction rate constant be accurately known.
This rate has been determined for the reverse direction by Lin,[2] who meas-
ured the electron density behind normal shock waves.

Exact numerical solutions for the expansion of non-equilibrium nozzle
flows have been obtained from a program developed at the Cornell Aero-
nautical Laboratory. These solutions indicate that over a wide range of
reservoir conditions the only important electron recombination mechanism
within the nozzle is the dissociative recombination reaction with NO$^+$.[1]
Consequently, by measuring the electron density in the nozzle of a hyper-
sonic shock tunnel the reaction rate constant can be determined by fitting
the numerical solution to the measurements.

The local temperature of the expanding air is determined by the
kinetics of recombination of the neutral species. This is seen in Table I
where the fraction of the total enthalpy of equilibrium air stored in dis-
sociation is tabulated. The reaction rates for the neutral species have
been extensively studied and Table II (taken from Reference 1) lists the
values used in the present study.

The amount of energy stored in vibrational modes is less than 10%
of the total enthalpy. However, the electronic temperature is coupled

to this vibrational temperature as indicated by chromium line reversal studies in hypersonic nozzle flows. The temperature of the free electrons will be determined by the electronic temperature since these collisions are most favorable for energy exchange to the free electrons.[3] Thus if the vibrational temperature froze in the nozzle, it may have an influence on the electron temperature. The electron recombination rate has an explicit dependency on the electron temperature and therefore the interpretation of measured electron densities as recombination rate constants is sensitive to the temperature history of the electrons.

The vibrational temperature in the nozzle was calculated by considering the vibrational relaxation of nitrogen. This species has the longest vibrational relaxation time of the air components and also contains most of the vibrational energy. The details of the calculation are given in Appendix A. The reservoir conditions considered varied from 5000 to 8000°K and 75 to 850 atm pressure. There was no appreciable vibrational nonequilibrium in the primary nozzle for pressures greater than 300 atm. For all reservoir conditions considered, the vibrational temperature froze as the flow passed through the expansion fan on the 10° deflection plate located between the primary nozzle exit and the conical nozzle entrance of the shock tunnel used for these studies. Since vibrational nonequilibrium is small over the range in which data were obtained, it will be assumed that all temperatures are in equilibrium with the local translational temperature of the gas.

A. Experimental Technique

The six-foot shock tunnel in which the ionization rates were measured is shown in Fig. 1. The driven tube, which is 28 feet in length and

3.00-inch inside diameter, is connected to a multi-stage nozzle system.
Figure 2 shows a detailed view of the nozzle system in partial section.
The two-dimensional expansion contour of the primary nozzle is designed
for wave cancellation for equilibrium airflow. A 10° flow-turning section
prevents solid particles from entering the second stage nozzle. The final
stage is a conical nozzle (10°-half angle) in which the flow expands to the
six-foot test section and receiver vessel shown in the foreground of Fig. 1.
The conical portion of the nozzle between the one-foot diameter station and
the six-foot test section is made of bonded glass fiber.

The microwave interferometer was used to measure the phase shift
and attenuation of electromagnetic waves due to propagation through the
plasma, which acts as a lossy dielectric medium. This technique has
been widely applied in gaseous discharge research and has been described
fully in the literature relating to that field (e.g. Refs. 4 and 5). Micro-
wave diagnostic methods are analogous to optical probes in that the pro-
pagating signal is so weak that it leaves the test gas essentially unperturbed.

Figure 3 shows a schematic diagram of the bridge circuit for the
interferometer. Power is supplied by a klystron oscillator through an
isolator in order to prevent reflected power from entering the oscillator.
A 3db directional coupler is employed to divide the power between the test
arm and the reference arm. Cross-guide couplers with crystal detectors
are mounted on either side of the test region in order to measure reflected
and transmitted power. Horns are used to transmit the microwaves through
the plasma. The reference arm is equipped with a phase-shifter and an
attenuator which are used both to initially balance the bridge and measure

5

the imbalance produced by the plasma. A detector is used to monitor power level in the reference arm. A magic-tee is used to mix the power from the two arms. The mixed signal is fed to the final detector through an isolator. Thus, the detected mixed signal is affected by attenuation and phase-shift in the plasma.

Figures 4 and 5 show the physical arrangement and location of the X-band microwave circuitry. The X-band transmitted signal is directed normal to flow direction through windows made of bonded glass fiber. The thickness of the windows was selected for optimal transmission of X-band (9397 Mc) microwave radiation. The test signal passes through the plasma in a region immediately downstream from the expansion fan which turns the flow through 10° and upstream from the entrance lips to the conical nozzle. The expansion fan introduces a slight nonuniformity in plasma properties which is perpendicular to both the flow and microwave beam. The magnitude of this gradient shows no more than a 4% variation about the mean electron density. Measurement of attenuation is more sensitive to this type of distortion than measurement of phase shift because of the directionality of the horns. However, auxiliary detectors situated at many locations failed to detect any refracted signal during the runs. Therefore, the flow is sufficiently uniform with the exception of the boundary layers on the windows. Boundary-layer growth in the primary nozzle was computed (for the range of conditions used) by means of a semi-empirical relationship given in Ref. 6. The calculated displacement thickness of the boundary layer on the fiberglass windows was approximately 0.1 of a free-space wavelength at 340 atm reservoir pressure while the total path length through the plasma is about four free-space wavelengths at X-band.

The S-band interferometer was located 38 inches downstream of the conical nozzle entrance lips, Fig. 4. The transmitted signal is perpendicular to the tunnel axis and passes through the fiberglass conical nozzle. The operating frequency (2890 Mc) was selected because it gave the minimum VSWR (voltage standing wave ratio). The boundary layer thickness was computed using the same empirical formula as was used for the primary nozzle. The displacement thickness of the boundary layer at the S-band interferometer location was 0.4 of a free-space wavelength at 340 atm reservoir pressure, while the inside nozzle diameter is four free-space wavelengths.

With no plasma present the interferometer was tuned to match out or the standing wave caused by multiple reflections between the horns. It is difficult to maintain this near-perfect tuning when a weak plasma is introduced because small alterations in the propagation path change the strength of the horns standing wave, and this produces either a loss or even a gain in the transmitted signal. Consequently, the measured attenuation is uncertain to $\pm$ 1 db. Before a test, the phase-amplitude bridge is nulled by adjusting the reference phase shift and attenuation until no signal is detected by the mixed signal detecting crystal. In order to test the tuning and the interaction between the two arms, carefully fitted polymer foam blocks having known dielectric and loss properties were placed between the windows in the nozzle. Measured phase shifts agreed with predicted values to with 10%. The shock tunnel, fitted with a closure plate which blanked-off the nozzle entrance, was operated at conditions typical of those used for nozzle runs. Interferometric data were then obtained to determine the disturbance levels of recoil motion and of elastic wave propagation. It was found that these mechanical effects

could be safely neglected in the interpretation of the data.

Microwave records were obtained for reference-arm power, plasma-reflected power, plasma-transmitted power, and mixed-signal power. The signal level through the reference arm remained constant during all runs indicating no unwanted interaction of this signal with the plasma in the test arm. The power reflection coefficient of the plasma was less than 0.1% for all experiments. The data were reduced to phase-shift readings by adjusting the phase-shifter and attenuator in the reference arm to duplicate the combination of transmitted power level and mixed signal level recorded at each time during the experiment. Attenuation due to the plasma could be obtained on the X-band interferometer because it was larger than the horn detuning effect described above.

Each phase-shift and attenuation record obtained first exhibited a sharp rise signifying the arrival of the leading compression wave which initiates the flow in the nozzle. The rise was followed by an irregular signal resulting from the tunnel starting process which was followed by a plateau having a comparatively low noise level. This plateau signified the useful, quasi-steady test flow of air. After the first plateau the ionization dropped to a second plateau at a level about one-half that of the first. Finally, the level dropped back to zero. The end of the useful test flow is marked by the first measurable effect of driver gas dilution of the air terminating the first plateau. It seems plausible that the second plateau arises from the nonequilibrium ionization frozen in the quenched combustion zone originating from an air-hydrogen diffusion flame sustained by interface mixing. A typical X-band interferometer record is shown in Fig. 6.

B. Data Analysis

The microscopic plasma properties, the electron plasma frequency f_p and the electron collision frequency f_c, can be calculated from the concentrations of the species that are present and the electron collision cross-sections.

The plasma frequency, which depends on the number density of the electrons, is given by

$$f_p^2 = n_e e^2 / \pi m$$

where n_e is the number density of electrons, e is the electronic charge, and m is the mass of the electron. The electron collision frequency is given by

$$2 \pi f_c = \frac{4}{3} \overline{V} \sum_j n_j Q_j$$

where $\overline{V}$ is the average electron speed, n_j is the number density of the jth species, and Q_j is the electron collision cross section with the jth species.

These microscopic plasma parameters are related to the macroscopic plasma parameters, dielectric constant ϵ and conductivity σ, through the equation of motion of a single electron. The resulting equations are

$$\epsilon = 1 - f_p^2 / (f^2 + f_c^2)$$

$$\sigma = \frac{1}{2} f_p^2 f_c / (f^2 + f_c^2)$$

where f is the microwave frequency.

For a uniform plasma the phase change and attenuation of a transmitted signal are given by

$$\phi_t = 2\pi(1-n)D$$

$$A = 2\pi K D \times 20 \log_{10} e$$

where ϕ_t is the change in transmitted phase when the plasma is intro-
duced, A is the attenuation of the transmitted signal in db's, and D is
the plasma thickness in units of the signal wavelength. The index of
refraction n and the extinction coefficient K are given by

$$2n^2 = \epsilon + \epsilon \left[1 + \left(2\sigma/f\epsilon\right)^2 \right]^{1/2}$$

$$2K^2 = -\epsilon + \epsilon \left[1 + \left(2\sigma/f\epsilon\right)^2 \right]^{1/2}$$

The loss of transmitted signal caused by reflections from the plasma boun-
daries can be neglected for the weak plasmas of this experiment.[7] To the
same approximation, n and K are given by

$$n \approx \epsilon^{1/2} \approx 1 - \sigma/f_c$$

$$K \approx \sigma/f$$

The ratio of attenuation to phase shift then depends only on the electron col-
lision frequency and bridge constants, but does not depend on the electron
density or the path length in the plasma.

In the present experiment the operating X-band frequency was 9375 Mc
which corresponds to a path length in the plasma of four wavelengths. For
electron densities greater than 3×10^{11} electrons/cc the attenuation becomes
so great that the interferometer is saturated. Therefore no electron den-
sities greater than this could be measured.

C.   Impurity Ionization

A major difficulty with any ionization experiment is the possibility of impurities with low ionization potentials contributing significantly to the electron density. This problem is even more acute in shock tunnel experiments because impurities ionized in the reservoir are probably monatomic (eg. Na^+) and therefore have only three-body recombination paths. At the relatively low densities of these experiments, the impurities will immediately freeze on expansion. Therefore the relative degree of impurity ionization is magnified by the expansion process since the air will be recombining.

A common impurity in shock tube spectroscopic studies is sodium which has a low ionization potential of only 5.12 ev. The equilibrium degree of ionization can be calculated from the Saha equation

$$\log_{10} n_e^2 / (n - n_e) = -5040 \, V/T + 1.5 \log_{10} T + 15.38$$

where

T = temperature in °K

V = ionization potential in ev.

n_e = electron density in particles/cc

n = atom density without ionization

The degree of ionization for sodium is shown in Fig. 7 for several initial atom concentrations. As can be seen, there is some temperature at which the sodium is completely ionized for each initial concentration. If it can be assumed that the impurity level is independent of the tunnel operating condition, then measurements made at low temperatures can be used to determine the impurity level for the higher temperature experiments.

To measure the impurity concentration, a series of runs were made with high purity neon as the test gas. Neon has a high ionization potential, 21.56 ev,

11

and therefore has a lower degree of ionization than air for the same temperature. Since neon is monatomic its chemical kinetics are quite simple. Electrons produced in the reservoir can only recombine during the expansion by three body processes. So the neon ions, like the impurity ions, will undergo a frozen expansion. Therefore, the expected electron density at the microwave interferometer locations can be calculated assuming no recombination. The correction to the area ratio due to boundary layer growth was obtained by assuming that the formula in Ref. 6 would still be approximately correct. The Mach number after the expansion fan becomes as high as 19.

The low reservoir temperature measurements in neon indicate an electron density of 1.4×10^9/cc, Fig. 8. The signal to noise ratio becomes very poor for low density measurements and introduces an error estimated at 1.5×10^9 electrons/cc. Consequently, the maximum impurity concentration in the reservoir scaled from this value is estimated to be 10^{12} atoms/cc. If the impurity were sodium, it would be fully ionized for reservoir temperatures greater than 3800°K.

The transmission through the plasma varied between attenuation and amplification for the low temperature runs. At the higher temperature of 7500°K the attenuation was 1.6 db. However, using the cross-section of neon,[8] the attenuation should have been much less. This indicates that most of this attenuation was caused by mismatch.

The electron density at the S-band interferometer location was consistent with the X-band data when boundary layer corrections were included. The attenuation of the S-band microwaves was 0.6 db. This implies that the electrons

were hotter than they were in the reservoir, therefore detuning effects accounted for most of the 0.6 db loss.

Runs identical to the neon runs were made in which argon was the test gas. The data, also shown in Fig. 8, substantiate the conclusions drawn from the neon data.

Assuming that the impurities have negligible effect on the ionization kinetics, then the measured electron densities in air can be used to determine the dissociative recombination rate constant of NO^+. Even if additional impurity sources existed when air was used, the low temperature air data indicates that at the higher temperatures the impurity contribution to the electron density can be neglected because the impurities would be fully ionized at 4000°K.

D. Error Estimates

The measured electron densities and collision frequencies are subject to a large number of errors. The measurements of the dielectric constant of foam blocks placed in the nozzle indicated a 10% error in phase shift. The insertion-loss measurements indicated an error of $\pm$ 1 db in attenuation. For most of the air runs, the X-band attenuation was approximately 10 db giving a 10% error due to this detuning effect. The oscilloscope records could be read to $\pm$ 5%. The calibration of these records in terms of phase shift and attenuation introduced another 5% error. The gradient of electron density in the boundary layers introduces an uncertainty in the effective path length. This could contribute as much as a 30% decrease in phase shift and 20% decrease in attenuation for the X-band interferometer.[9] For the S-band interferometer location the boundary layer is thicker,

introducing an estimated 60% error in phase shift. This conservatively assumes that the electron boundary layer is the same order as the gas density displacement boundary layer. The total error is then 50% for phase shift and 40% for attenuation for the X-band interferometer.

The uncertainty in the electron density measured by the X-band interferometer is then $\pm$ 40%. The collision frequencies obtained are more accurate since for a weakly reflecting, underdense plasma they are proportional to the ratio of attenuation and phase shift and independent of path length. Therefore the collision frequencies will not be as greatly affected by the electron density gradients. Consequently the electron collision frequencies as measured by the X-band interferometer are accurate to $\pm$ 25%.

For the S-band interferometer the attenuation ($<$ 2db) was the same order as the losses due to detuning effects. Therefore no reliable values for the collision frequencies could be obtained. Fortunately the electron density for a low loss plasma is determined primarily by the phase shift and is not sensitive to attenuation. The uncertainty in the electron density is therefore $\pm$ 80%.

E. <u>Deionization Rate Constant</u>

The electron density at a given area ratio in nonequilibrium expanding airflows is relatively insensitive to reservoir pressure, but is almost inversely proportional to the rate constant,[10] (Fig. 9). Estimates of the electron density were obtained from numerical solutions of nonequilibrium nozzle flows for reservoir temperatures from 5000°K to 8000°K at a few typical reservoir pressures. The calculations were performed using the computer program described in Ref. 11 and the neutral particle kinetic data shown in

Table II. Reaction 10 was the only ionization reaction considered for the reasons given previously. A polynomial curve-fit of the geometric area function of the primary nozzle contour was employed. Boundary-layer corrections based on the methods of Ref. 6 were applied to obtain the gas-dynamic conditions at the exit of the nozzle; this correction never exceeded 3%. The electron mass concentration at the geometric exit area was used. This is a better approximation than the effective area because the slope of the area function is small near the exit. Hence, the integrated residence time would be more nearly described by choosing the nonequilibrium ionization level based on actual axial distance rather than the axial distance corresponding to effective area ratio.

Since the concentration of the neutral particles was essentially frozen at the conditions of the experiment, ideal gas calculations were employed for obtaining conditions after the expansion fan which turns the flow through 10°. Frozen vibration was also assumed to obtain the effective specific heat ratio. Ionization relaxation was calculated for the inner and outer streamlines bounding the microwave beam. The outer streamline was approximated by line segments with an average density for the expansion fan. Computation of ionization relaxation for the inner streamline was straightforward since the residence time in the expansion fan is approaching zero. Over-all reductions in electron mass concentrations between primary nozzle exit and X-band microwave beam were approximately 30% for all cases. More recombination along the outer streamline than the inner streamline resulted in a plasma gradient which was mutually perpendicular to the flow velocity and the microwave propagation direction. As mentioned previously, this

15

variation never resulted in nonuniformity exceeding 4% about the mean value. The extent of recombination in the expansion fan was rather insensitive to the computational model; therefore, no higher approximations for the outer streamline were sought.

For the flow in a conical nozzle when the neutral species concentrations have frozen, the electron mass concentration can be given analytically by[12]

$$\gamma_e = const \Big/ x^{2n(\eta-1)-1}$$

where

γ_e = electron density in moles/gm mixture

x = axial distance from cone apex

n = temperature exponent of recombination rate constant

η = frozen specific heat ratio

The electron densities measured by the interferometers are shown in Figs. 10 and 11. The maximum electron density determined from the X-band interferometer is 3×10^{11}. At reservoir temperatures above 6000°K many runs indicated a greater electron density, these could not be quantitatively measured because the attenuation exceeded 14 db which saturated the interferometer.

Additional data points were obtained which are not shown. These data point fell below those shown and were rejected for three reasons. First, if they were correct then the temperature dependency of the recombination rate would be -3.0, this is double the theoretical limit established by Bates.[13] Secondly, the measurements made in neon and argon flows

indicated that there was no high density source of impurity ionization which could cause the higher recorded level. Third, for the run records which indicated the higher electron densities the second plateau level corresponded to the lower level of ionization. This would indicate that for those runs which only showed the lower ionization level, there was not a finite testing time in air uncontaminated with driver gas. The loss in testing time for high enthalpy shock tunnels can also be seen from the aerodynamic data.

For a reservoir temperature of 6000°K and a reservoir pressure of 340 atm, the electron density at the conical nozzle inlet (X-band interferometer location) varies from 1 to 3 times 10^{11}, the average value being 1.75×10^{11} electrons/cc. At the S-band interferometer location the average value is 4.5×10^9 electrons/cc. The boundary layer correction to the density ratio between these two locations depends on the reservoir pressure. For a 340 atm reservoir pressure the ratio is 23. Therefore the ratio of electron mass concentrations is

$$\left(\gamma_e\right)_s \Big/ \left(\gamma_e\right)_x = \left(n_e \big/ \rho\right)_s \left(\rho \big/ n_e\right)_x = 0.59$$

The effective specific heat ratio is 1.41. The location of the X-band interferometer is $x = 18.9$ cm and for the S-band $x = 115.9$ cm. Therefore the temperature exponent is -1.60. This is very close to the value usually assumed of -1.5. Because of the data spread the value of -1.5 will be used. The complete rate constant determined from Fig. 9 is then $3 \times 10^{20} T^{-1.5}$ cc/mole sec. This value is lower by a factor of 6 then that determined by Lin from measurement behind normal shock waves in air.[2,14] This difference is remarkably small because Lin measured this rate in the direction of electron production whereas we have measured it in the direction of

17

electron removal. These rates are related by the law of mass action when local equilibrium is assumed. Refinements in the theoretical interpretation of both sets of experimental data which include the possible existence of intermediate species (eg. NO^*) and correct electron energy distribution functions may bring both rate constants into complete theoretical agreement.

F. Electron Collision Frequency

The electron collision frequencies were obtained from the X-band interferometer records. The large uncertainty in the S-band attenuation precluded any collision frequency determination. The predicted collision frequencies are shown in Fig. 12 for the electron temperature equal to the local gas translational temperature. The atom and molecule cross-sections used for predicting the electron collision frequencies in Fig. 12 are shown in Fig. 13.[15] The species concentrations were taken from the nonequilibrium nozzle flow solutions with appropriate boundary layer corrections.

The insensitivity of the predicted collision frequencies to reservoir pressure and temperature occurs because the nitrogen molecule concentration is approximately constant at 2.6×10^{-2} moles/gm of mix (five times that of any other species) over the entire range of conditions considered.

The measured collision frequencies are higher by a factor of six than the predicted collision frequencies. The collision frequencies varied from 2×10^9 to 2×10^{10} cps, i.e. from $f^2 \gg f_c^2$ to $f_c^2 > f^2$. This difference can not be accounted for by corrections to the collision frequency which include electron-ion collisions, 2×10^7 cps, electron-sodium atom collisions, 10^4 cps (assuming 10^{13} atoms/cc in the reservoir), and electron-copper atom collisions, 10^7 cps (assuming 0.1 cc of nozzle throat is vaporized,

an extreme upper limit). For those runs which only showed the lower

ionization level, the corresponding collision frequency was nearly the

same as those shown in Fig. 12. Addition experiments are in progress

which will measure the cross-section of N_2.

II. COLLISION CROSS-SECTION MEASUREMENTS

The electron collision frequency in a plasma is determined by the energy distribution of the electrons and by the collision cross-sections of the other plasma species. Measurements of the collision cross-sections of O_2 and N_2 are summarized in Ref. 15. The cross sections of O and N have not been directly measured, however, the theoretical values have been given by Klein and Brueckner[16] which agree with photodetachment cross-sections.

A few of the experimental measurements have employed microwave diagnostic techniques. The high electron temperatures were obtained by some form of RF heating. Consequently the neutral species were at room temperature while the electrons had some assumed velocity distribution function. The experimental results, presented in Section I of this report, indicate that the collision frequency in a plasma whose neutral species are at a high temperature is greater than would be expected on the basis of the previously measured cross-sections. This experiment cannot be regarded as conclusive because of questions concerning the relaxation of internal energy modes, which at present are not fully understood.

The determination of the correct collision cross-sections to electrons in a hot thermal plasma can best be done by measuring the collision frequency in a well-defined equilibrium plasma so that questions concerning the energy distribution do not arise. Consequently the technique which is being employed is to perform microwave diagnostic measurements in the equilibrium plasma produced behind normal shock waves in a shock tube.

A. Instrumentation

The microwaves are propagated axially up the shock tube where they interact with the advancing plasma behind the shock wave. The microwave parameters which are measured are the reflected power, the transmitted power, and the transmitted phase change. The arrangement of the microwave equipment is schematically the same as in the interferometer used on the shock tunnel (Fig. 3). The only differences are that the transmitting horn is replaced by a waveguide taper to change the waveguide dimensions from the standard size to the 1-1/2 x 2-1/2 inch shock tube dimensions and the receiving horn is replaced by a specially designed coupler in the broad wall of the shock tube.

The end wall of the shock tube is a quartz block 1-1/2 x 2-1/2 x 1.308 inches cemented to the shock tube side walls. The VSWR of this block has two minimums in the X-band frequencies. The one occurs at a frequency of 11590 Mc with a VSWR value of 1.09 and the other at 9320 Mc with a VSWR of 1.07. The function of the quartz block is to permit the transmission of the microwaves into the shock tube but to prevent the shock wave from entering the microwave circuitry.

An experimental study of the reflection of microwaves from an over-dense plasma in this shock tube has already been reported.[7] The operating X-band frequency for that study was 9375 Mc. Although higher order modes were present, they contained less than 1% of the power. In the present experimental program the interferometer has been operated at 11590 Mc. At this higher frequency additional modes can propagate in the shock tube. The results to date indicate than an appreciable percentage of the power may

21

be in the higher modes. However, tuner and isolators in the external circuitry have greatly reduced the erratic ripple in the recorded data. The optimum design has not yet been found.

It may be necessary to make the collision frequency measurements at the frequency of 9320 Mc to avoid the higher mode problem. This has not been done to date because the high power X-band klystron (see Section III) operates only at this frequency. For the high-power interaction experiment it is desirable to have simultaneous diagnostic measurements so the interferometer needs to be used at 11590 Mc.

B.   Data Interpretation

There are three advantages to using axial microwave propagation as opposed to cross-channel measurements. The first is that within the waveguide the fundamental mode is strictly a plane wave incident on the plasma at an angle determined only by the operating frequency and the shock tube dimensions. Therefore, plane wave theory (given for example in Stratton[17]) can be used for data reduction. The second advantage is that the thickness and location of the plasma are continually changing in a known and predictable way. Therefore, the effects of mismatching and higher modes can be separated from the time variation of the recorded data. The third advantage is that the length of the uniform, equilibrium plasma must only be large enough to produce measureable effects. There is no requirement that it be large compared with, for example, the transmitting and receiving cross-channel horns. This allows the shock tube to be operated at low pressures (low collision frequencies) with no restrictions imposed by the testing time loss which occurs as the pressure level is

22

decreased. [18,19]

The range of plasma conditions over which the interferometer can be operated is determined on the high temperature side by the requirement that the plasma be underdense so that transmission measurements can be made. The lower limit will be imposed by the noise level of the interferometer. For an operating frequency of 11590 Mc, the critical electron density is 1.68×10^{12} electrons/cc. Figure 14 shows the equilibrium electron density in pure oxygen and nitrogen plasmas. The relative atom to molecule concentration is shown in Fig. 15. At low densities oxygen becomes almost completely dissociated. Therefore, measurements of the collision frequency can be used to determine the oxygen atom cross-section. For nitrogen the situation is not as favorable because of the higher dissociation energy. It does not seem that the cross sections for atomic nitrogen can be determined unless diagnostic measurements are made at a frequency of at least 70 kMc or the cross section of atomic nitrogen is very large.

III. HIGH-POWER INTERACTION

When high-power microwaves interact with a thermal plasma they cause a modification of the plasma. First, the energy distribution function of the electrons is changed. This can cause the collision frequency of electrons to increase, thereby decreasing the attenuation of signals through an overdense plasma. Second, the electron density can increase and may cause breakdown of an underdense plasma. Third, the distribution of the neutral species in their various energy states can be altered. This will modify the optical signature of re-entry vehicles.

A. Instrumentation

A high-power X-band transmitter (the property of Contract AF-30(602)-2267) may be available for the interaction studies. This transmitter can deliver a continuous 4 kw signal at 9350 Mc to the shock tube. This signal will enter the shock tube in the axial direction simultaneous with the low power probing signal at 11590 Mc. Separation of the signals in the external microwave circuitry is achieved by narrow band pass filters (diplexer). By using the probing signal the changes produced in the electron collision frequency and in the electron particle density can be determined from either transmission or reflection measurements. The examination of the changes in population distribution of the neutral species will be made with spectroscopic techniques.

B. Spectroscopic Observations

Oxygen and nitrogen molecules are both homonuclear, therefore vibrational and rotational transitions in a given electronic state are strictly forbidden. For nitrogen, transitions to the ground state from any other

electronic state are also forbidden. In oxygen, transitions to the ground state from the $B\ {}^{3}\Sigma_{u}^{-}$ state are allowed (Schumann-Runge bands). However the overlap integrals (Frank-Condon factors) are small below $\nu'' = 12$. None of these difficulties exist with the nitric oxide gamma bands, however these bands are spectrally overlapped by the oxygen Schumann-Runge bands. At the temperatures necessary to produce ionization some of the nitric oxide will have decomposed into oxygen.

If theoretical considerations should indicate that observation of the ground state vibrational levels must be made to understand the electron-neutral particle energy exchange mechanism, then these levels could be monitored from Raman spectra. A long duration laser beam could be used as the source of incident radiation. It may, however, be sufficient to monitor only those bands which have already been successfully studied in the shock tube[20-23] with the instruments available in this laboratory.

IV. CONCLUSIONS

The deionization rate in air has been measured in the CAL six-foot shock tunnel. This tunnel can produce reservoir temperatures of over 7000°K, however, above 5000°K the testing time varies drastically from run to run. This shock tunnel is presently going to be modified to increase the testing time and thus allow operation at higher enthalpy levels. The modified tunnel can then be used to verify the present results and to extend them to higher enthalpies where several more reactions began to become important.

The electron density at two different nozzle stations has been measured. From these data the reaction rate for dissociative recombination reaction of NO^+ has been determined. The temperature dependence of the reaction rate was found to be -1.60 or 7% greater than the usually assumed value of -1.5. This difference is not significant because of spread in the data. The pretemperature factor was found to be 3×10^{20} with an uncertainty of a factor of two. The measured rate constant for $NO^+ + e^- \longrightarrow N + O$ is then taken to be $3 \times 10^{20} \, T^{-1.5}$ cc/mole-sec. This rate is lower than the value obtained from shock tube measurements; however, within the quoted accuracies they do agree. The difference in the rate constants may be real because of different electron energy distributions or the formation of intermediate compounds.

The electron collision frequency was also determined. The measured values were substantially higher than the predicted values. The difference could not be attributed to errors in boundary layer growth or impurities. However, shock tube experiments are in progress to resolve this anomaly.

APPENDIX A

ELECTRON TEMPERATURE IN THE SIX-FOOT SHOCK TUNNEL

The determination of the electron recombination rate from electron density measurements in a hypersonic nozzle requires that the electron temperature in the nozzle be known. In the reservoir the electrons are assumed to have a Maxwellian velocity distribution at the gas temperature.

The gas translational temperature in the nozzle can be determined from the nonequilibrium expansion computer program. The electron temperature is then found from

$$\frac{dE_e}{dt} = \sum_i G_i \nu_i \left(E_i - E_e\right)$$

where

E_e = electron energy = $3/2\ kT_e$

E_i = energy of ith species

G_i = inelastic fractional energy loss

ν_i = collision frequency

In terms of the fluid velocity u, the equation becomes approximately

$$\frac{\Delta T_e}{\Delta x} = \sum_i \frac{T_i - T_e}{L_i}$$

where $L_i = \dfrac{u}{G_i \nu_i}$ and $E_i = \dfrac{3}{2} k T_i$

For the condition of the present experiment the electron temperature will always equal the local gas temperature.

Computations were performed for nitrogen vibrational relaxation to determine if the vibrational temperature stayed in equilibrium with the translational temperature. This was done because the electron temperature may be more strongly coupled through electronic excitation to vibrational temperature

than to translational temperature.

For an harmonic oscillator the vibrational energy is given by

$$E_v = \frac{R_0\,\theta_v}{e^{\theta_v/T} - 1}$$

where θ_v = 3353°K for nitrogen. The relaxation equation is

$$\frac{dE}{dx} = \frac{\bar{E} - E_v}{L}$$

where $\bar{E}$ is the vibrational energy evaluated at the local translational temperature and L is $u\,\frac{(\tau p)}{p}$ where p is the nitrogen pressure and (τp) is the "vibrational relaxation time". In the calculations p was taken as the local static pressure since nitrogen is the major constituent and (τp) was found by using the theoretical curve in Fig. 1 of Ref. 24.

Near equilibrium we can put

$$\frac{dE}{dx} = \frac{d\bar{E}}{dx}$$

then

$$E_{v_2} = \bar{E}_2 - \frac{L_1}{\Delta x}\left(\bar{E}_2 - \bar{E}_1\right)$$

where the numerical subscript indicates the station where the quantity is evaluated. When the relaxation length exceeded 1 cm, it was assumed that

$$\frac{dE}{dx} = \frac{dE_v}{dx}$$

then

$$E_{v_2} = E_{v_1} + \left(\bar{E}_1 - E_{v_1}\right)\frac{\Delta x}{L_1}$$

The calculations for a reservoir pressure of 75 atm indicate that the nitrogen vibrational temperature would freeze in the first stage nozzle for reservoir temperatures between 5000 and 7000°K. At 850 atm the vibrational temperature did not freeze until the flow started the rapid expansion around the turning wedge.

REFERENCES

1. Eschenroeder, A. Q., Daiber, J. W., Golian, T. C. and Hertzberg, A., Shock Tunnel Studies of High-Enthalpy Ionized Airflows, CAL Rept. No. AF-1500-A-1, July 1962.

2. Lin, S. C., Neal, R. A. and Fyfe, W. S., Rate of Ionization Behind Shock Waves in Air. I. Experimental Results, AVCO Res. Rept. 105, September 1960.

3. Gaydon, A. G. and Hurle, I. R., The Shock Tube in High Temperature Chemical Physics, Reinhold, New York (1963), pp. 212, 219.

4. Goldstein, L., Electrical Discharges in Gases, Advances in Electronics, Vol. 7, p. 399, 1955.

5. Wharton, C. C., Microwave Diagnostics for Controlled Fusion Research, Plasma Physics, Chap. 12, J. E. Drummond, Ed., McGraw-Hall Publishing Co., New York, 1961.

6. Burke, A. F. and Bird, K. D., The Use of Conical and Contoured Expansion Nozzles in Hypervelocity Facilities, CAL Rept. No. 112, January 1962 (based on paper presented at the Second National Symposium on Hyper-velocity Techniques, Denver, Colo., March 19-20, 1962).

7. Daiber, J. W. and Glick, H. S., Plasma Studies in Shock Tube, Proc. of the Symposium on Electromagnetics and Fluid Dynamics of Gaseous Plasma, Poly. Inst. Brooklyn, April 4-6, 1961.

8. Brown, S. C., Basic Data of Plasma Physics, John Wiley & Sons, New York, 1959.

9. Albini, F. A. and Jahn, R. G., Reflection and Transmission of Electro-magnetic Waves at Electron Density Gradients, Jour. Appl. Phys. 32, 75, 1961.

10. Eschenroeder, A. Q. and Daiber, J. W., Nonequilibrium Ionization in Shock Tunnel Flows, ARS Journal 31, 94, 1961.

11. Eschenroeder, A. Q., Boyer, D. W. and Hall, J. G., Nonequilibrium Expansions of Air with Coupled Chemical Reactions, CAL Rept. No. AF-1413-A-1, AFOSR 622, May 1961; Phys. of Fluids 5, 615, 1962.

12. Eschenroeder, A. Q., Ionization Nonequilibrium in Expanding Flows, ARS Journal 32, 196 (1962).

13. Bates, D. R., Dissociative Recombination, Phys. Rev. 78, 492, 1950.

14. Lin. S. C. and Teare, J. D., Rate of Ionization Behind Shock Waves in Air. II Theoretical Interpretation, AVCO Res. Rept. 115, September 1962.

15. Shkarofsky, I. P., Bachynski, M. P. and Johnston, S. W., Collision Frequency Associated with High Temperature Air and Scattering Cross-Sections of the Constituents, Electromagnetic Effects of Re-entry. Pergamon Press, 1961.

16. Klein, M. M. and Brueckner, K. A., Interaction of Slow Electrons with Atomic Oxygen and Atomic Nitrogen, Phys. Rev. 111, 1115, 1958.

17. Stratton, J. A., Electromagnetic Theory, McGraw-Hill, 1941, p. 500.

18. Roshko, A., On Flow Duration in Low-Pressure Shock Tubes, Phys. Fluids 3, 835, 1960.

19. Hooker, W. J., Testing Time and Contact-Zone Phenomena in Shock-Tube Flows, Phys. Fluids 4, 1451, 1961.

20. Daiber, J. W. and Williams, M. J., Transition Probabilities for Nitric Oxide in the Far Ultraviolet, J. Quant. Spectrosc. Radiat. Transfer. 1, 135, 1962.

21. Wurster, W. H., Treanor, C. E. and Thompson, H. M., Nitric Oxide Bands Near 1μ in Shock-Heated Air, CAL Rept. No. QM-1626-A-6, June 1962.

22. Wurster, W. H., Measured Transition Probability for the First-Positive Band System of Nitrogen, CAL Rept. NO. QM-1626-A-3, January 1962.

23. Wurster, W. H. and Treanor, C. E., Transition Probabilities for O_2 Radiation in the Near Ultraviolet, CAL Rept. No. QM-1209-A-1, August 1958.

24. Stollery, J. L. and Smith, J. E., A Note on the Variation of Vibrational Temperature Along a Nozzle, J. Fluid Mech. 13, 225, 1962.

ACKNOWLEDGEMENTS

32

TABLE I
FRACTION OF THE ENTHALPY OF EQUILIBRIUM AIR STORED IN DISSOCIATION

TEMP.	PRESSURE	
°K	.100 atm	1000 atm
5000	.203	.094
6000	.273	.160
7000	.334	.210
8000	.428	.268

TABLE II
KINETIC DATA FOR REACTIONS OF NEUTRAL SPECIES

$$K_{Fi} = A_i T^{n_i} \exp(-\theta_i/T) cm^3 \, mole^{-1} \, sec^{-1} \text{ FOR T IN °K}$$

i	REACTION	COLLISION PARTNER, M	A_i	n_i	θ_i
1	$O_2 + M \underset{K_{B_i}}{\overset{K_{F_i}}{\rightleftharpoons}} 2O + M$	O_2	3.6×10^{21}	-1.5	59380
2		O	2.1×10^{18}	-0.5	59390
3		N_2	1.2×10^{21}	-1.5	59380
4	$N_2 + M \rightleftharpoons 2N + M$	N_2	3.0×10^{21}	-1.5	113260
5		N	1.5×10^{22}	-1.5	113260
6		O_2, O, NO	9.9×10^{20}	-1.5	113260
7	$NO + M \rightleftharpoons N + O + M$	N_2, O_2, O N, NO, Ar	5.2×10^{21}	-1.5	75490
8	$N + O_2 \rightleftharpoons NO + O$		1.0×10^{12}	0.5	3120
9	$O + N_2 \rightleftharpoons NO + N$		5.0×10^{13}	0	38000
10	$e^- + NO^+ \rightleftharpoons N + O$				0

34
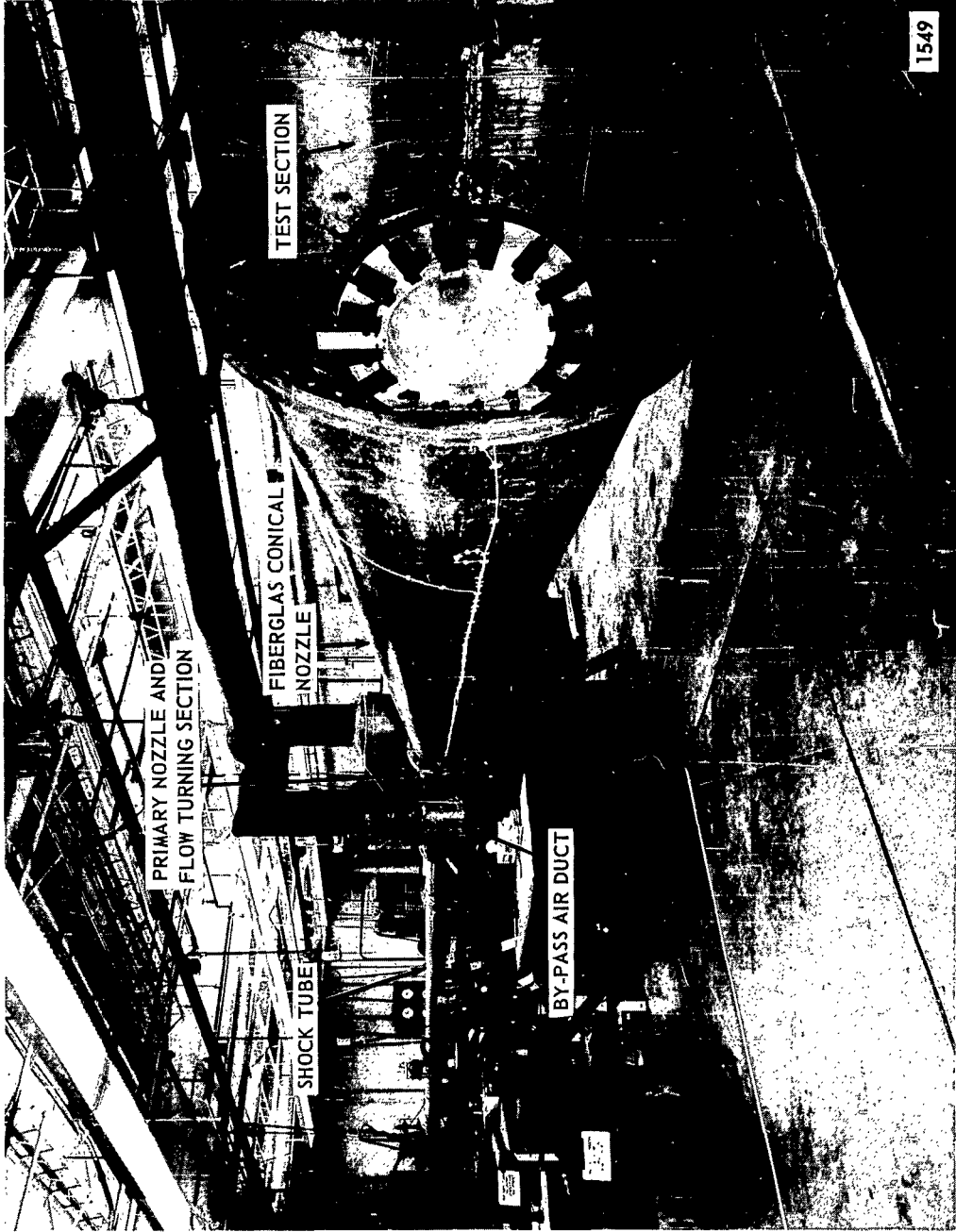
Figure I   PHOTOGRAPH OF THE CAL 6 FOOT HYPERSONIC SHOCK TUNNEL

TERMINAL
NOZZLE

ELECTION

1816
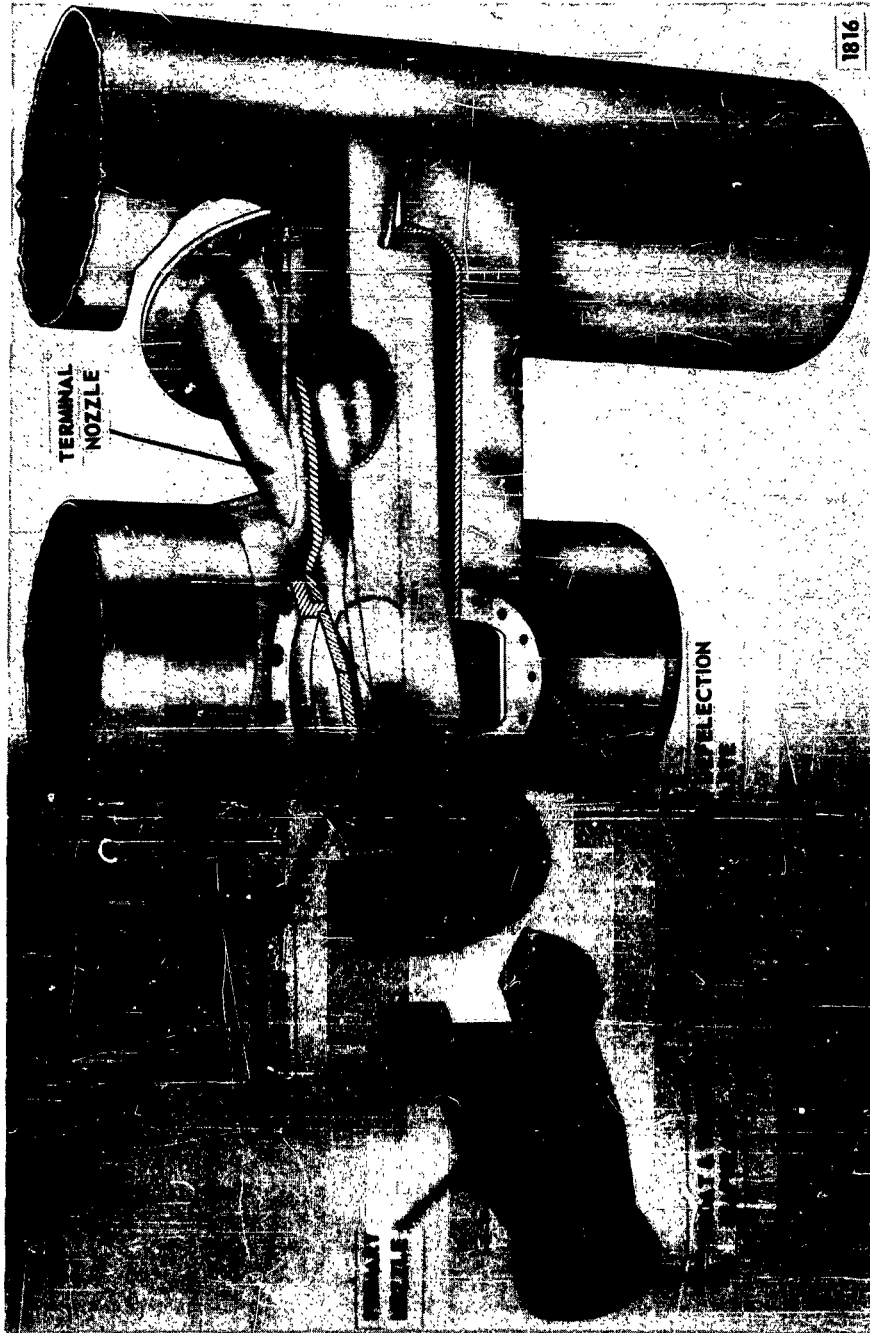
Figure 2 PRIMARY NOZZLE, FLOW-TURNING SECTION, AND CONICAL NOZZLE ENTRANCE
FOR THE CAL 6 FOOT HYPERSONIC SHOCK TUNNEL
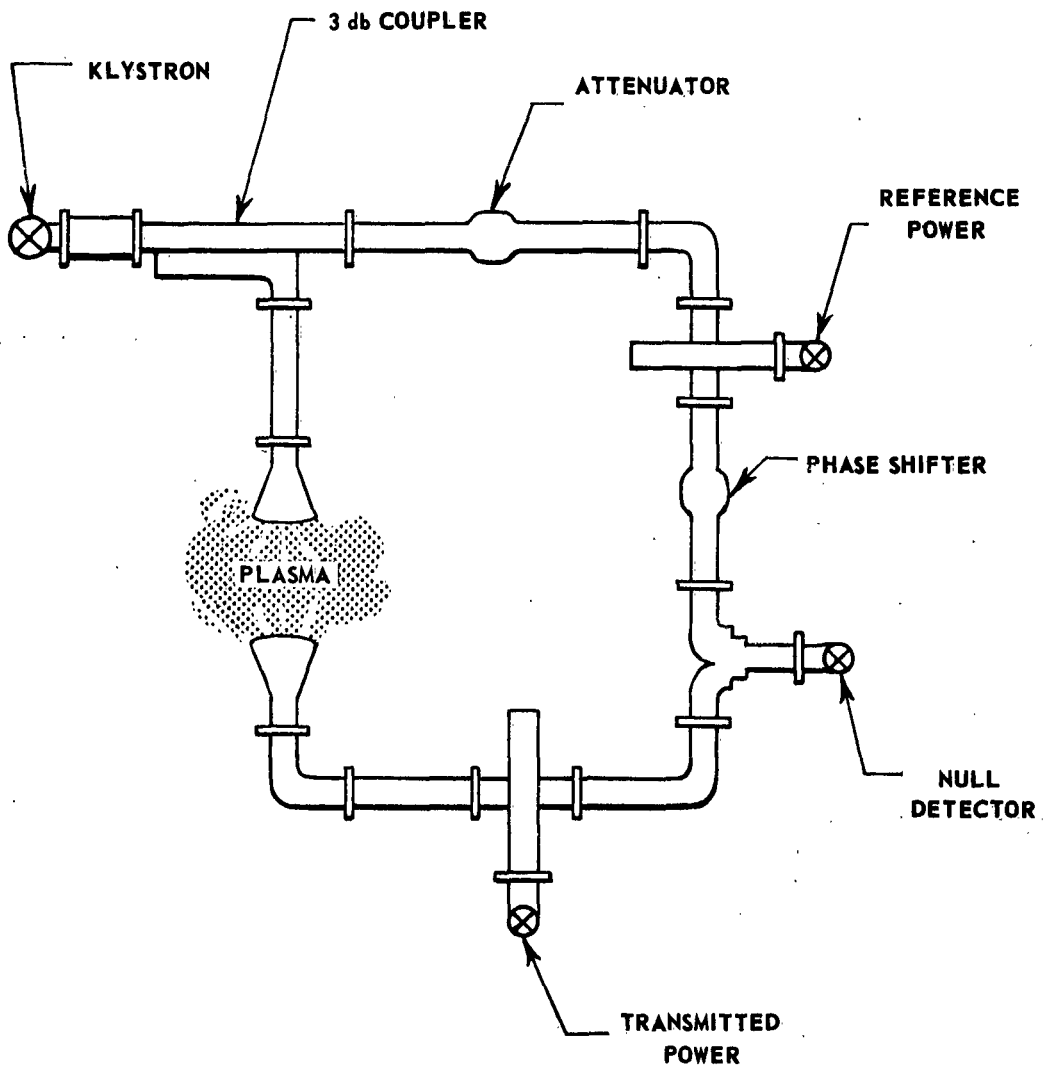
Figure 3 MICROWAVE INTERFEROMETER SCHEMATIC
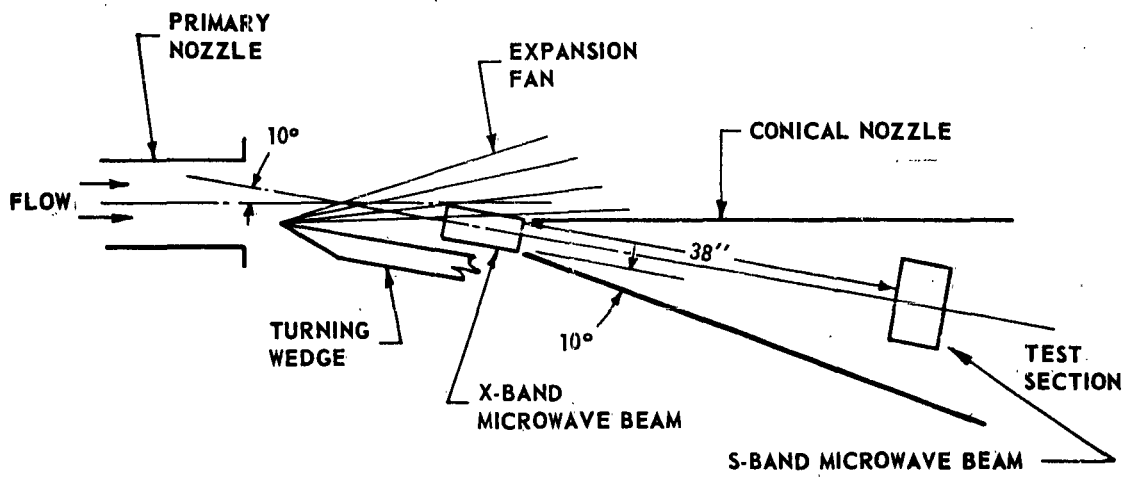
Figure 4 MICROWAVE INTERFEROMETER LOCATIONS
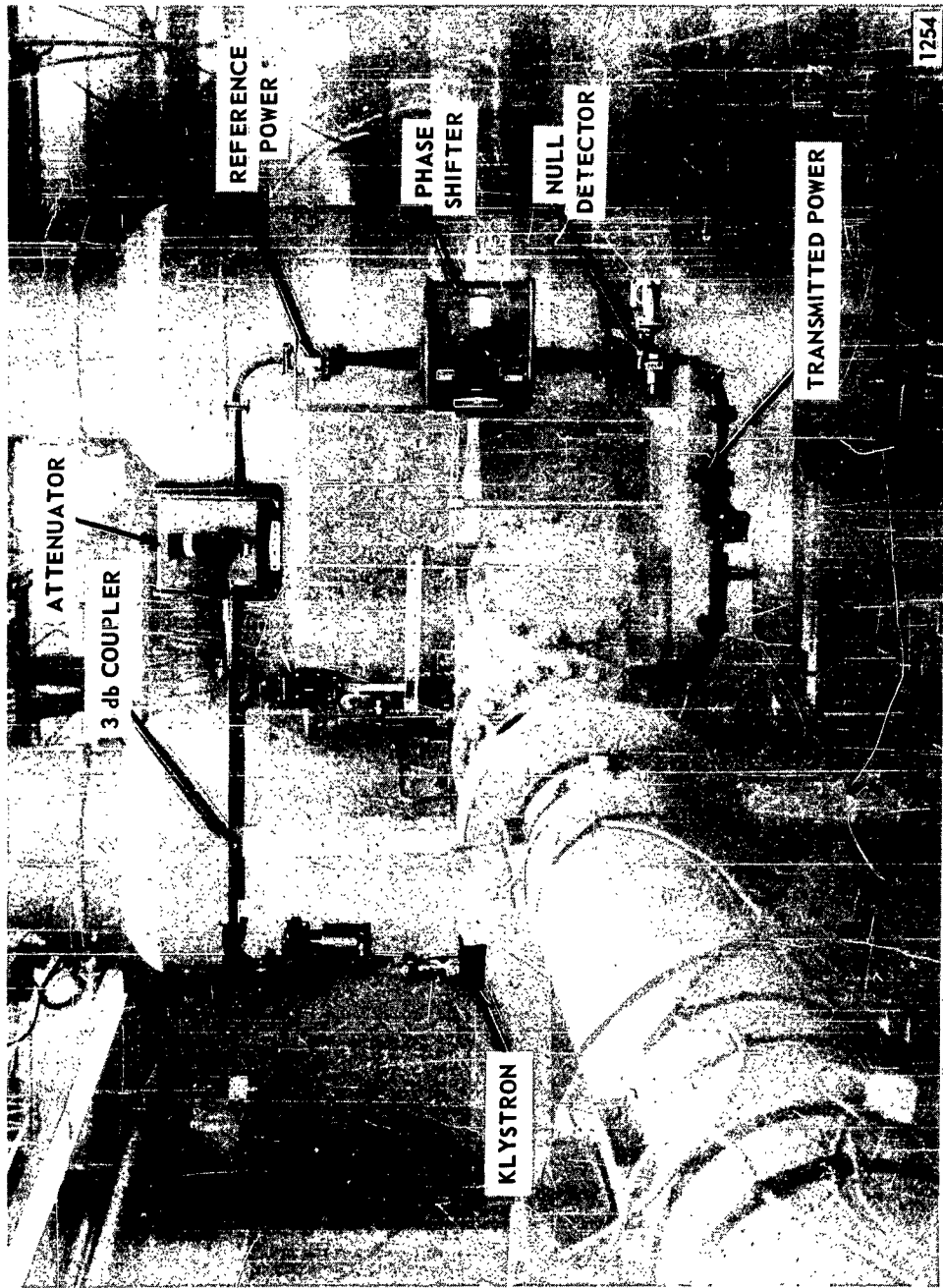
Figure 5   PHYSICAL ARRANGEMENT OF THE X-BAND MICROWAVE INTERFEROMETER
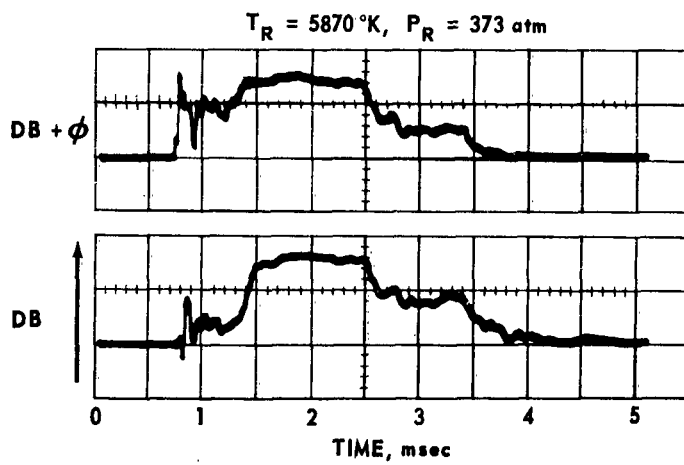
Figure 6   TYPICAL X-BAND INTERFEROMETER RECORD
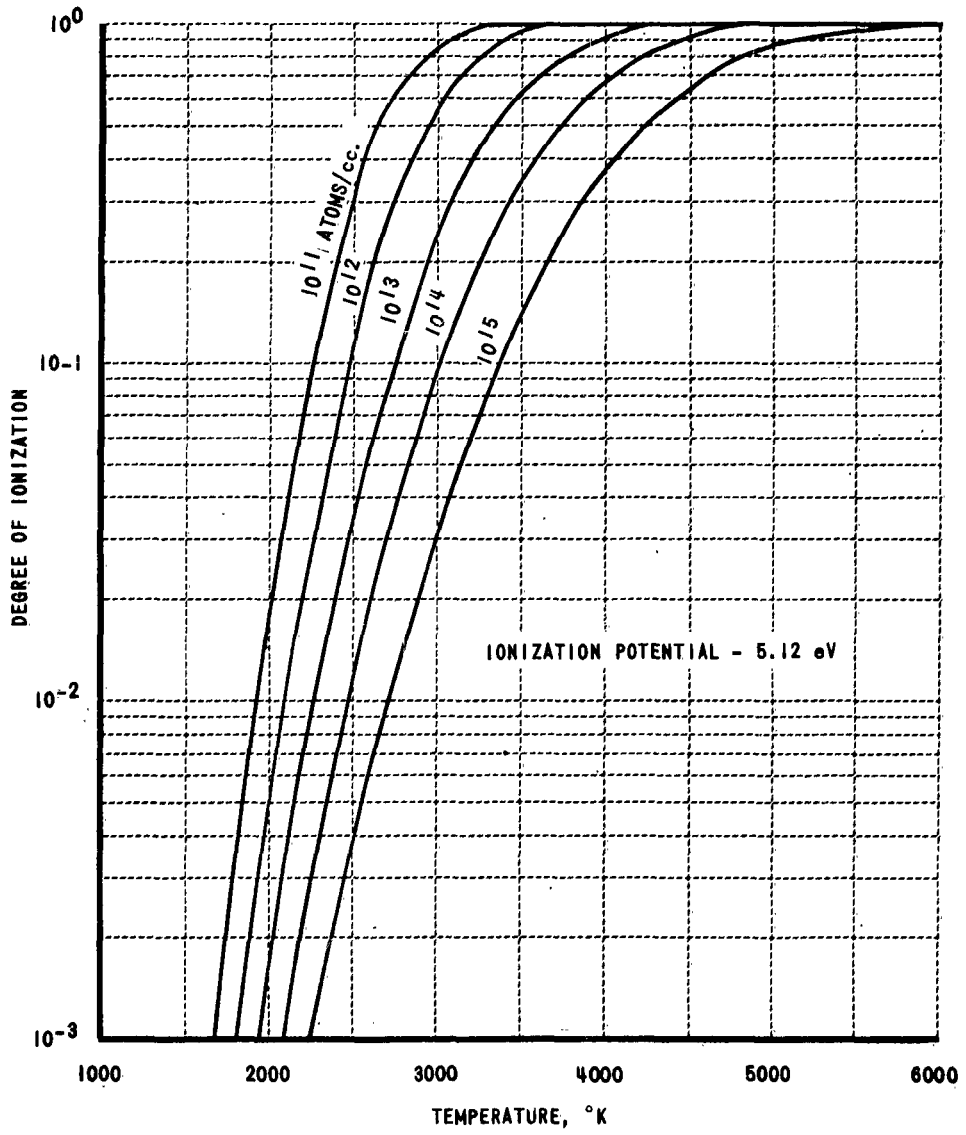
Figure 7   EQUILIBRIUM DEGREE OF IONIZATION OF SODIUM
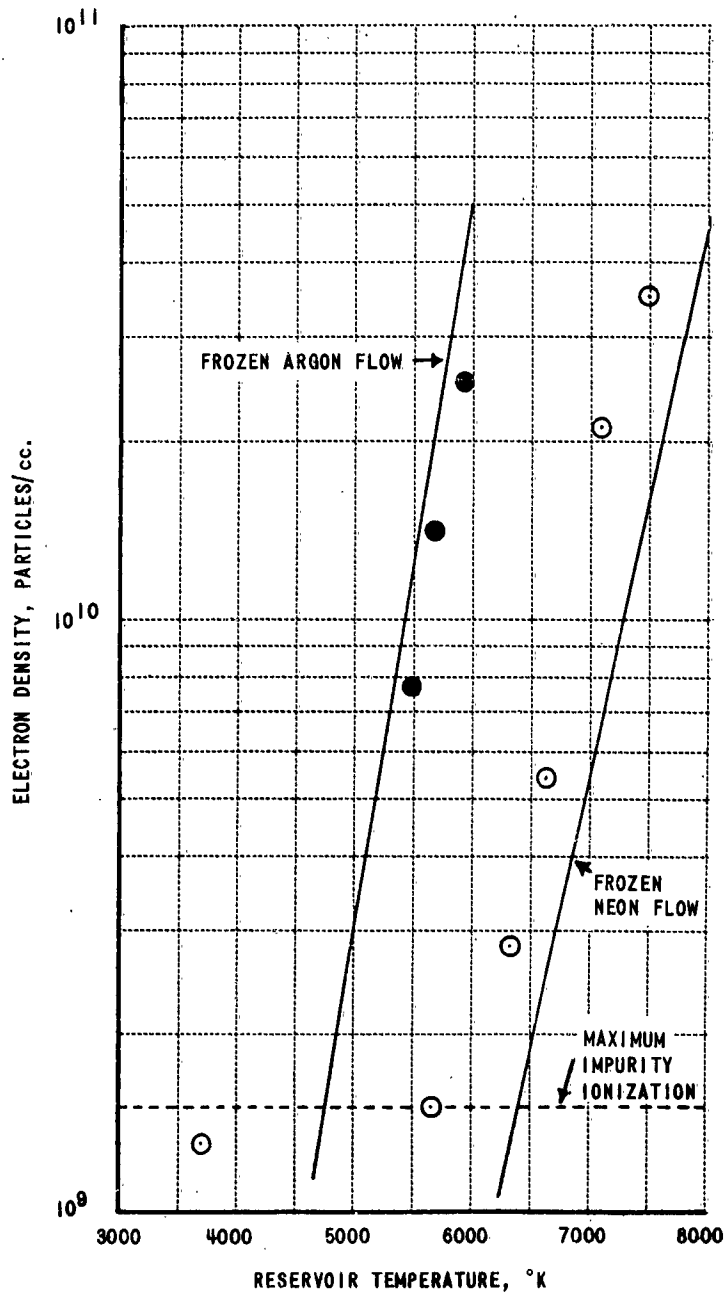
Figure 8   ELECTRON DENSITIES AT THE CONICAL NOZZLE INLET FOR ARGON AND
NEON FLOWS
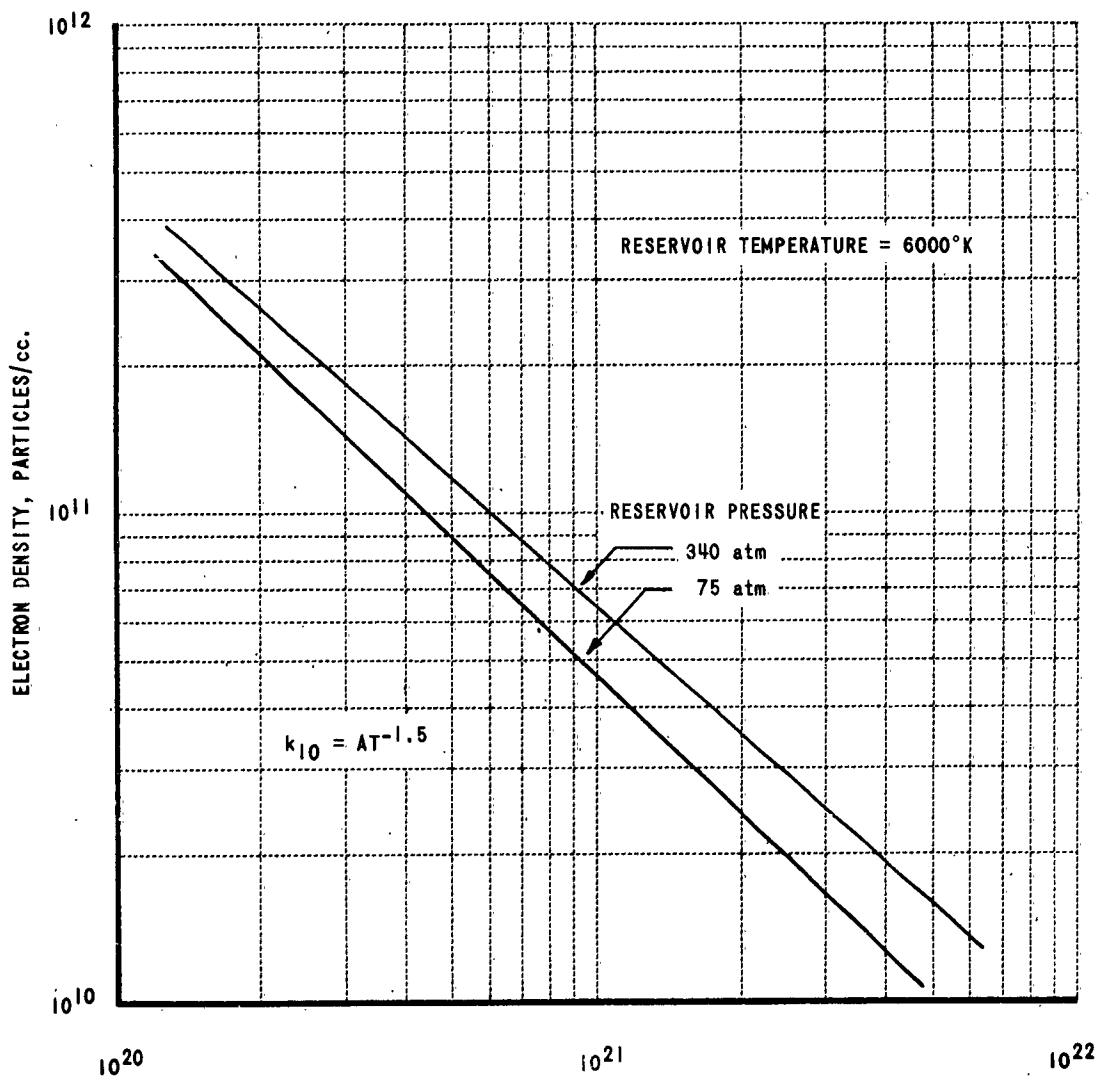
Figure 9 PREDICTED ELECTRON DENSITIES AT CONICAL NOZZLE INLET
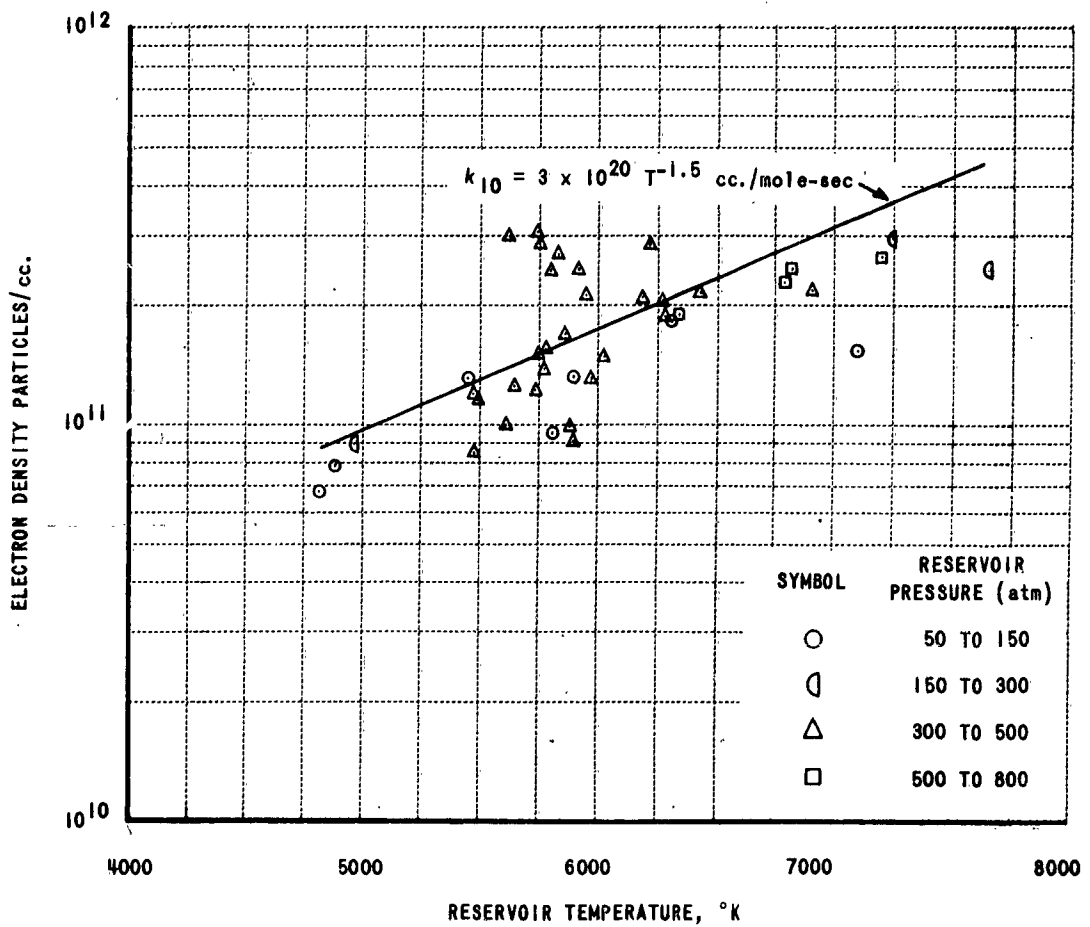
Figure 10 ELECTRON DENSITIES MEASURED BY THE X-BAND INTERFEROMETER
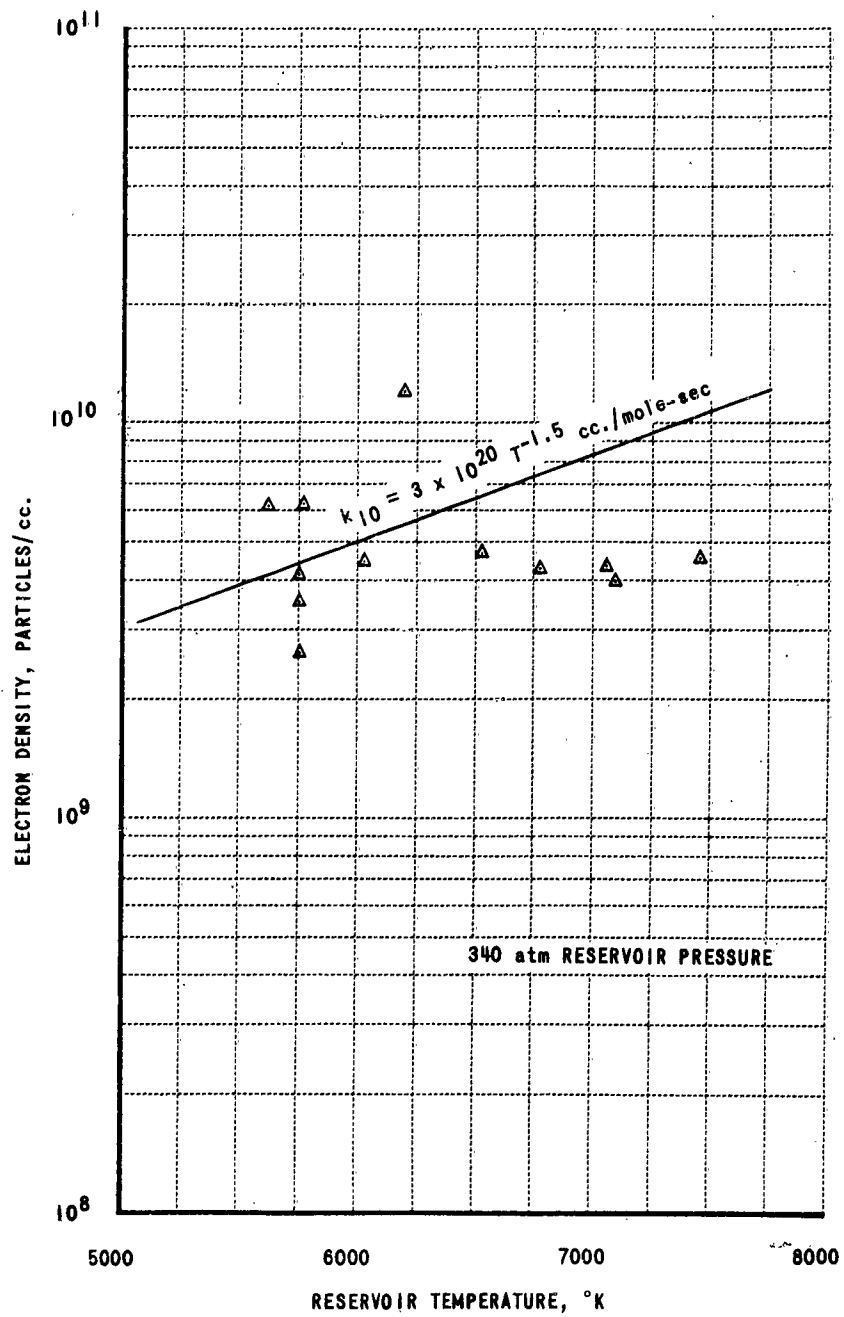
Figure 11   ELECTRON DENSITIES MEASURED BY THE S-BAND INTERFEROMETER
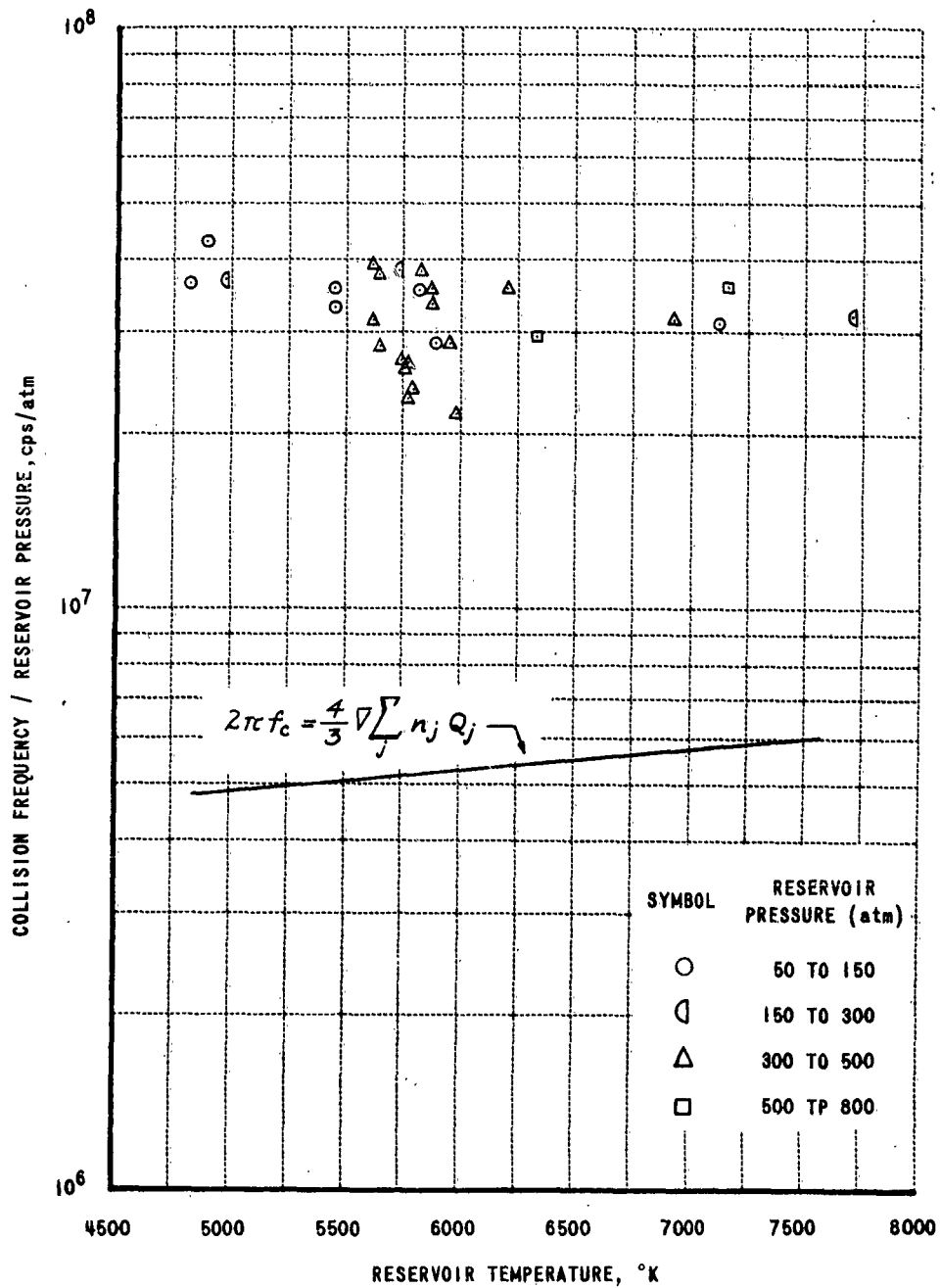
Figure 12 ELECTRON COLLISION FREQUENCIES AT THE CONICAL NOZZLE INLET
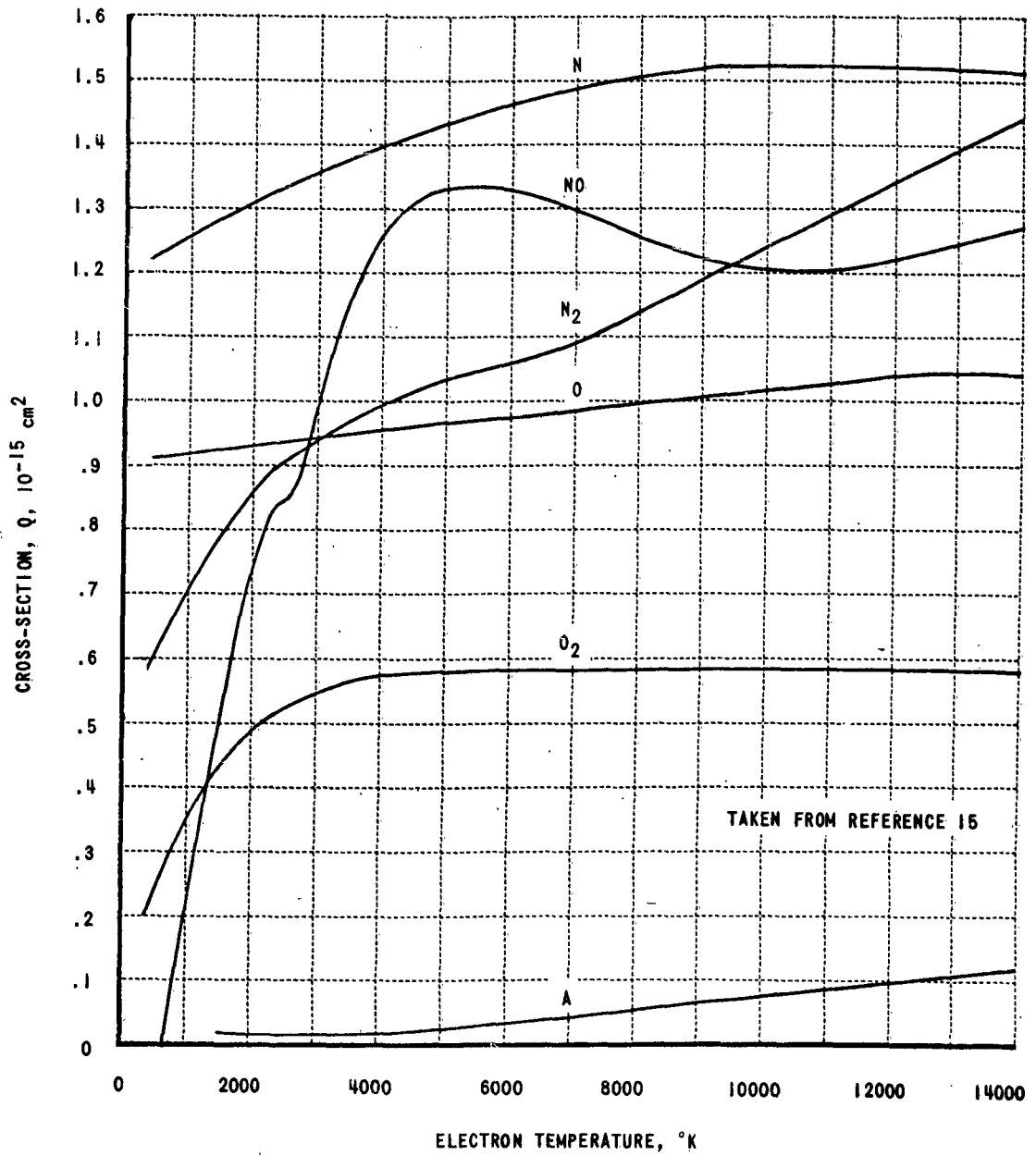
Figure 13   ELASTIC COLLISION CROSS-SECTIONS
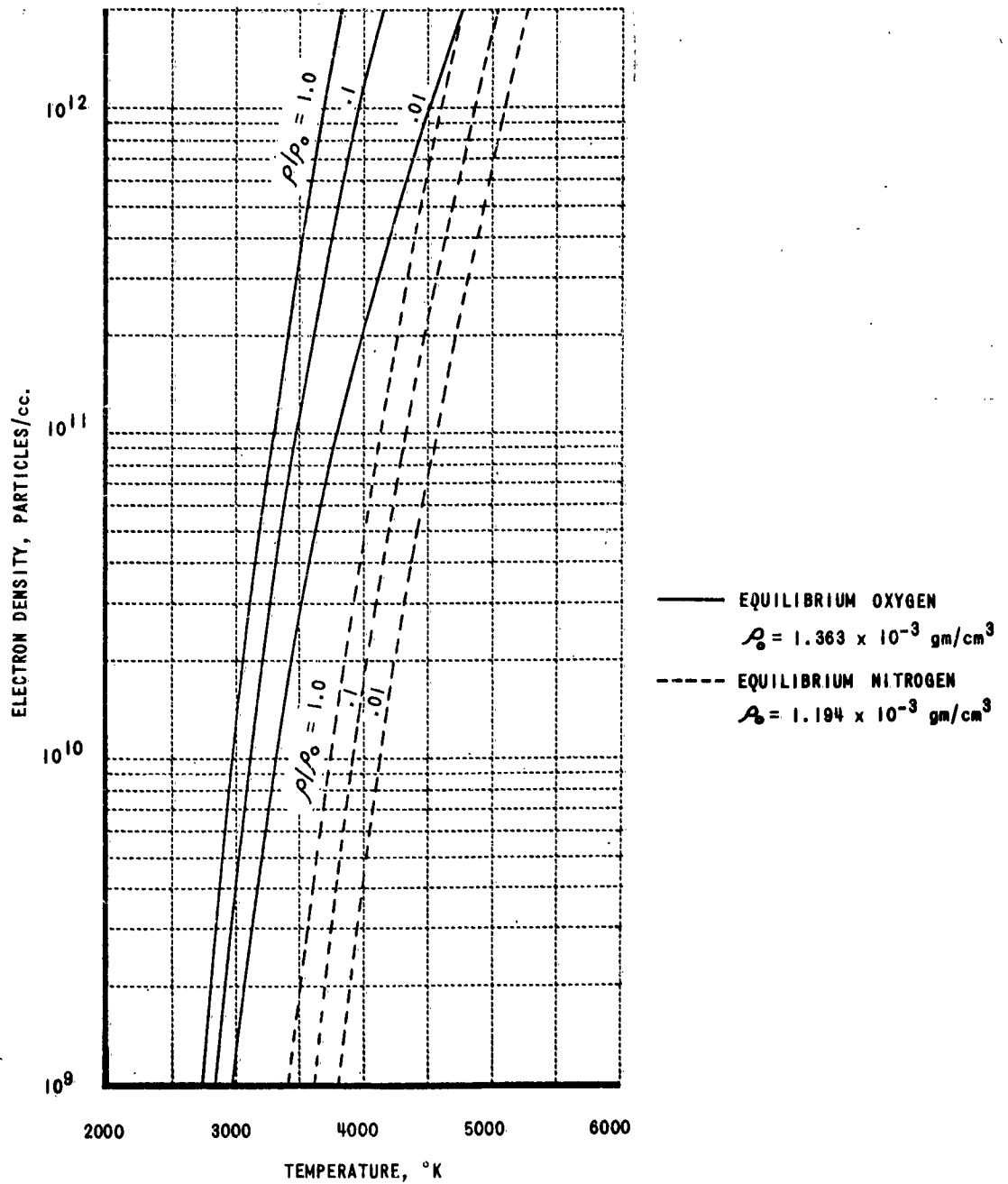
Figure 14 ELECTRON CONCENTRATION IN EQUILIBRIUM OXYGEN AND
NITROGEN PLASMAS
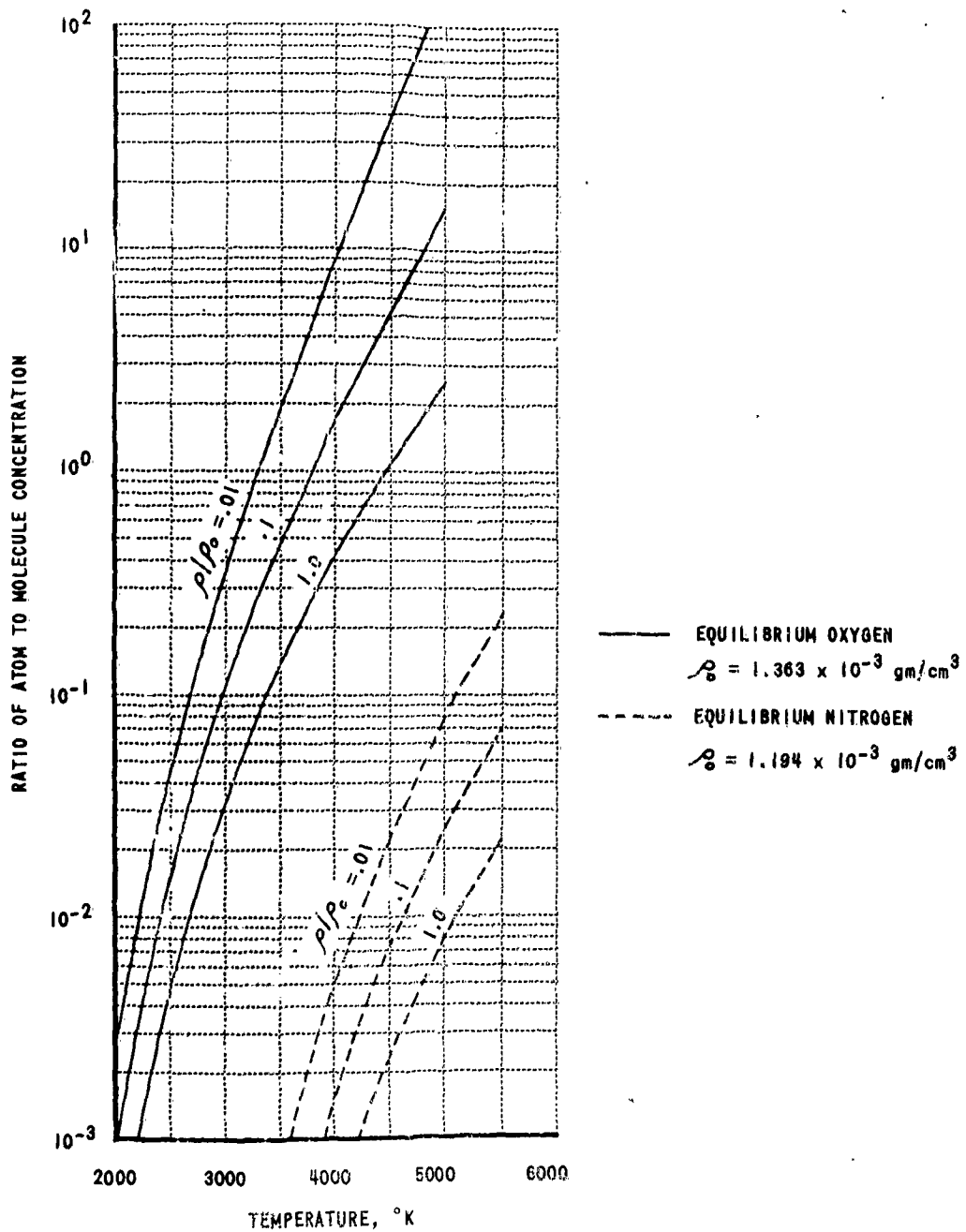
Figure 15 RELATIVE ATOM AND MOLECULE CONCENTRATIONS IN EQUILIBRIUM
OXYGEN AND NITROGEN PLASMAS